1971 "SILVER MEDAL" BRITISH ACOUSTICAL SOCIETY ADDRESS
delivered at the 1972 SPRING MEETING of the Society at

The University of Loughborough.

THE ACOUSTICS OF AXIAL FLOW MACHINES

by Dr.C.L.Morfey, Istitute of Sound
and Vibration Research.

1. INTRODUCTION

The study of axial flow machines from an acoustical viewpoint can be said to have begun with Gutin [1, 2], whose 1936 paper on propeller noise was the basis of most of the advances made during the next twenty years. Since then, Lighthill's development of aerodynamic sound theory [3], and in particular Curle's extension of the theory in 1955 to include solid boundaries [4], have been recognised as providing a more general foundation for further work in this field.

The essential step taken by Lighthill was to incorporate into a linear acoustic model the nonlinear features of aerodynamic sound generation This led to the vamous V^8 law for high-speed jet noise; but was initially disregarded in the work on aircraft turbomachinery noise which followed in the 1960's. An account of some of the early Rolls-Royce work in this field was given in 1964 by Bragg and Bridge [5]; the sound produced by axial flow compressors was attributed to fluctuating blade forces, mainly on the grounds of a V^6 dependence on blade speed.

More recently it has been recognised [6,7] that particularly for high speed subsonic machines, Lighthill's full acoustic analogy predicts additional sources of sound which may be significant; and that in supersonic machines, where a shock pattern propagates away from the rotor inlet (or exit) plane, an important part of the noise spectrum is due to nonlinear wave propagation, which the analogy with linear acoustics is ill-suited to describe. Nonlinear propagation effects fall outside the scope of the present paper, whose aim is to review the applications of linear acoustic theory to subsonic turbomachinery. Within this limitation, however, the various source mechanisms indicated by the acoustic analogy are discussed in some detail.

Particular attention is given to simplified models from which straightforward analytical predictions may be obtained. There are two reasons for adopting such an approach. The first is the insight gained from a simple result, provided, of course, it is not so simplified as to miss the main point. Secondly, from an experimental viewpoint, there seems little virtue in using

more elaborate theories during the present rather primitive stage of interpreting noise measurements.

Comparisons between the theoretical predictions and measured data are made in the final section, under three general headings :

(a) effect of flow on sound radiation from known sources;
(b) radiation from a blade row operating in a known non-uniform flow;
(c) relation between sound power output and steady-flow operating parameters.

2. AERODYNAMIC SOUND THEORY

Internal flows in turbomachinery are inherently unsteady, and this unsteadiness coupled with the compressibility of the working fluid leads to sound generation. The coupling process was first described by Lighthill [3], for a flow without boundaries. In turbomachinery, on the other hand, solid boundaries are present in the form of blades and play an essential part in the generation of sound.

The complexities introduced by the presence of solid boundaries cannot be avoided in any general treatment of turbomachinery noise. They arise for two reasons. The first is purely acoustical: given an acoustic source distribution in the region external to the blades, the resulting sound field is scattered by the blade surfaces. The second is more fundamental: the acoustic analogy implicit in the previous statement may be rendered useless by the presence of solid surfaces in the sound-generating flow.

2.1 Limitations of the acoustic analogy for aerodynamic sound

The acoustic analogy idea, in the form originally given by Lighthill [3], consists of regarding the density , ρ, in the actual flow as being driven by a source distribution, q, in a fictitious uniform fluid at rest. The value of q is simply the value of $(\partial^2\rho/\partial t^2 - c_o^2\nabla^2\rho)$ as given by the equations of motion of the real fluid; c_o is the sound speed in the fictitious fluid. The usefulness of this idea in practice depends on whether q can be specified to sufficient accuracy without knowing the solution for ρ in advance.

In the case of unsteady compressible flow over solid surfaces, no such foreknowledge of q is in general available. The reason is that the normal-velocity boundary condition provides a strong coupling between q and ρ. Methods have been developed for dealing with this situation, and are described in Section 6; but the essential simplicity of the acoustic analogy is lost. Fortunately, however, it is possible to neglect the coupling between q and ρ in the limit of blade chords, ℓ, small compared with the sound wavelength, λ. Also, if $\ell \ll \lambda$, the acoustic problem of scattering by blades is greatly simplified. Results based on this approximation are given in Section 5.

2.2 The acoustic analogy for high Reynolds number flows

Since the practical application of the acoustic analogy is to the case $\ell \ll \lambda$, it is convenient to replace the blades by applied-force and displacement distributions which reproduce the boundary conditions on the blade surfaces. (Heat transfer to the fluid is neglected). In this way, an acoustic analogy is obtained with an unbounded fluid, as was originally proposed by Curle [4].

Distributed sources are therefore introduced as follows [8]: a volume displacement z per unit volume, together with force components ρg_i (i=1,2,3) per unit volume applied to the fluid. The displacement effect of blades is represented by a volume displacement rather than by introduction of new fluid, since the latter does not correspond to the physical situation.

Introduction of the volume displacement z leads to a two-fluid continuum model, in which unit volume of space contains mass $\rho(1-z)$ of the real fluid. The dynamics of the fictitious fluid occupying the displaced volume are of no interest; it is simply necessary to specify continuity of pressure with the surrounding real fluid (here assumed inviscid and non-conducting). The equations of motion for the actual fluid are

$$\frac{Ds}{Dt} = 0 \; ; \tag{1}$$

$$\frac{\partial V_i}{\partial x_i} = \frac{1}{1-z} \frac{Dz}{Dt} - \theta_p \frac{Dp}{Dt} \; ; \tag{2}$$

$$\frac{DV_j}{Dt} = \frac{g_j}{1-z} - \frac{1}{\rho(1-z)} \frac{\partial p}{\partial x_j} \; . \tag{3}$$

The equation of state of the fluid is taken as

$$\ln\rho = \theta(p,s) \qquad (4)$$

and partial derivatives of θ are indicated by subscripts.

For internal flows it is convenient to base the acoustic analogy on a uniform fluid which is not at rest (as was chosen by Lighthill) but in uniform motion, with velocity components U_i. A second, and less trivial, departure will be made from Lighthill's approach by choosing p rather than ρ as the acoustic variable; this is important if the flow contains entropy inhomogeneities (hot spots), since the corresponding density perturbations are not propagated as sound waves. Thus the objective is a convected wave equation of the form

$$\frac{1}{c_o^2}\left(\frac{\partial}{\partial t} + U_i \frac{\partial}{\partial x_i}\right)^2 p - \nabla^2 p = q \,, \qquad (5)$$

with q expressed in terms of the flow variables (V_i, p, s, z, g_i).

The nature of q in equation (5) is clarified by considering a special case . If the actual flow departs only infinitesimally from the reference state of uniform motion, and there are no external sources, it is well known that pressure perturbations in an inviscid non-conducting fluid are described by equation (5) with q=0. Contributions to q arise, in this case, only from nonlinear interactions between the various perturbations [9].

An approximation for the analogous acoustic source strength q, in terms of $v_i = V_i - U_i$, $p' = p - p_o$, $s' = s - s_o$ and the external source terms, has been given in [8]. It is based on equations (1) to (4) with the following simplifications,

(a) Products of the external source terms are omitted. For describing sound generation by interacting blade rows, this is justified on the ground that source distributions which represent different blade rows do not overlap.

(b) Third order products of the quantities listed above are neglected, if they explicitly contain z or g_i.

(c) Third order products which contain p' (either explicitly or in the form $\partial v_i/\partial x_i$) are also neglected.

The result may be written as

$$q = \rho_o \frac{\bar{D}^2 z}{Dt^2} - \rho_o \frac{\partial g_i}{\partial x_i} + \Delta q \qquad \left(\frac{\bar{D}}{Dt} \equiv \frac{\partial}{\partial t} + U_i \frac{\partial}{\partial x_i}\right) , \tag{6}$$

where Δq represents a set of nonlinear interaction terms :

$$\Delta q \doteq \rho_o \frac{\partial^2 v_i v_j}{\partial x_i \partial x_j} - (\rho\theta_s)_o s' \frac{\partial^2 v_i v_j}{\partial x_i \partial x_j}$$

$$- \frac{1}{2}\rho(\theta_{pp} + \theta_p^2) \frac{D^2}{Dt^2}(p'p') - \rho\theta_{ps} s' \frac{D^2 p'}{Dt^2} - \frac{\partial}{\partial x_i}\left(\theta_s s' \frac{\partial p'}{\partial x_i}\right)$$

$$+ \rho\theta_p \frac{D^2}{Dt^2}(p'z) - \rho\theta_p \frac{\partial}{\partial x_i}(p'g_i) . \tag{7}$$

For a perfect gas with specific-heat ratio γ, the thermodynamic derivatives occurring in (7) are given by

$$\theta_p = \frac{1}{\rho c^2} = \frac{1}{\gamma p} \quad ; \quad \theta_s = -1/C_p , \tag{8}a$$

and (assuming γ constant)

$$\theta_{pp} = -\gamma\theta_p^2 \quad ; \quad \theta_{ps} = 0 . \tag{8}b$$

2.3 Application to axial flow machines

The acoustic analogy as set out in equations (5) to (7) may be used to estimate the radiated sound from various high Reynolds number unsteady flows. Perhaps the best-known application is Lighthill's theory of turbulent-jet noise, in which the first term of Δq was identified as an equivalent source. In hot subsonic jets, the second term is likely to be important. Finally in nonlinear acoustics, Westervelt has used the first and third terms to describe sum and difference frequency radiation from intersecting sound beams [10], and has shown how the last two terms describe nonlinear effects at a radiating surface [11].

When applied to the flow around blades in subsonic turbomachinery, the acoustic analogy indicates a number of possible sound sources. These are listed below against the corresponding source terms in (6) and (7).

(a) $\rho_o \bar{D}^2 z/Dt^2$, $-\rho_o \partial g_i/\partial x_i$: (i) Thickness and steady loading of rotating blades [1,2]. (ii) Unsteady blade forces, due to pressure or vorticity disturbances acting on a blade row.

(b) $\rho_o \partial^2 v_i v_j/\partial x_i \partial x_j$: (i) Interaction between velocity fields of fixed and moving blade rows; the individual velocity fields may consist either of blade wakes or the blade-to-blade potential velocity variation. (ii) Interaction of turbulence, or other flow distortions, with the velocity field of a rotor [6].

Because this source is of quadrupole order, while the corresponding blade forces give rise to a dipole term, it is unimportant at low Mach numbers.

(c) $s'\partial^2 v_i v_j/\partial x_i \partial x_j$ term : Entropy wakes or hot spots interacting with the velocity field of a rotor. Such interactions will occur in turbines if there is non-uniform combustion, or in fans if there is a non-uniform heat source upstream.

(d) $(s'p')$ terms : One of these vanishes if the fluid is a perfect gas, while the other is of dipole order. The previous term (c) is therefore more important at low Mach numbers.

(e) $(p'p')$, $(p'z)$, $(p'g_i)$ terms : Interactions between the pressure field of one blade row and the pressure field, thickness or loading of another. At low Mach numbers these sources are insignificant compared with the unsteady blade forces which occur.

3. FREE-FIELD ROTOR MODELS

Once an equivalent acoustic source distribution has been found using the acoustic analogy, the problem is one of solving the linear convected wave equation with appropriate boundary conditions. A free-field model is appropriate for unducted propellers and rotors and its application is discussed briefly below.

3.1 Ring source radiation

Gutin in 1936 developed a theory of propeller noise in which the blade thickness and loading were represented by source distributions in the propeller disk [1,2]; this amounted to a primitive version of the acoustic analogy later developed by Lighthill. Gutin's work led to the useful idea of a ring source distribution, which was taken up by Embleton and Thiessen [12] and subsequently in more detail by Wright [13]. Besides forming a basic element from which a finite rotor disk may be constructed, the ring source with linear circumferential phase variation displays most of the important properties of free-field rotor radiation. In addition, if the blade span is less than the acoustic wavelength, a single ring source at a mean radius can adequately represent the entire rotor (provided the circumferential phase speed of the source pattern is supersonic).

A simple-source ring distribution (Figure 1) is defined by

$$q = \mathrm{Re}\ \bar{A}\, e^{i(m\phi-\omega t)}\, \delta(r-a)\delta(x)\ , \quad (m=0,\pm1,\pm2 \text{ etc}); \qquad (9)$$

the source is positioned at ($r=a$, $x=0$) in the cylindrical co-ordinate system (x,ϕ,r). Equation (9) defines a single-frequency source with linear circumferential phase variation. If the surrounding acoustic medium is at rest ($U_c = 0$), the far-field pressure amplitude at the point (R,θ,ϕ_o) in Figure 1 is

$$\bar{p} = i^{-m} e^{im\phi_o}\, \frac{e^{ikR}}{R}\, .\, \frac{1}{2}a\, \tilde{A}\, J_m\,(ka \sin\theta)\ , \quad (k=\omega/c_o). \qquad (10)$$

An immediate deduction from equation (10) is that for subsonic circumferential phase speeds - which according to (9) occur when $|ka/m| < 1$ and $m \neq 0$ - the sound field is relatively weak. Physically, this is because of cancellation between out-of-phase regions of the source; mathematically, the effect is contained in the Bessel function factor in (10).

Of greater practical significance for rotor noise is the corresponding solution for a ring force distribution, where the force per unit volume applied to the fluid is given by

$$\mathrm{Re}\ (\bar{P}, \bar{Q}, \bar{R})\, e^{i(m\phi-\omega t)}\, \delta(r-a)\delta(x)\ . \qquad (11)$$

$\bar{P}$, $\bar{Q}$ and $\bar{R}$ are the amplitudes of the force per unit circumference in the x, ϕ and r directions. The far-field pressure follows from (10), by differentiating with respect to the source position co-ordinates [14]:

$$\bar{p} = i^{-l-m} e^{im\phi_0} \frac{e^{ikR}}{R} \cdot \frac{1}{2} \{(ka \cos\theta.\bar{P} + m\bar{Q})J_m + \frac{1}{2}ika \sin\theta.\bar{R}(J_{m-1}-J_{m+1}$$

(12)

The Bessel functions in (12) all have argument ka sin θ, as in (10). The same remarks about subsonic phase speeds apply as to the simple-source result.

Physically, a subsonic rotor can give rise to a supersonically rotating source pattern only if it operates in a circumferentially distorted flow. Such flow distortions are therefore extremely important in determining the radiated sound field.

3.2 Radiation from point forces in circular motion

If the blades on a rotor are small compared with the sound wavelength, the unsteady loading on each blade is adequately represented by a single point force with components (T, D, C). The corresponding ring force distribution due to a single blade is therefore

$$(P, Q, R) = (T, D, C) \cdot \frac{1}{a} \delta(\phi-\phi_1) \quad , \qquad (13)$$

where $\phi_1 = \Omega t + \phi_1'$ is the angular position of the blade in question. Once the variation of T with ϕ_1 is specified, for example as

$$T = \mathrm{Re}\ \bar{T}\, e^{-i\lambda\phi 1} \quad , \qquad (14)$$

equation (13) can be Fourier analysed to give the circumferential harmonic amplitudes $\bar{P}$; similarly for the other components, $\bar{Q}$, $\bar{R}$.

Any periodic variation of the blade forces may be represented by a combination of harmonic terms as in (14). A rotor operating in a steady distorted flow, for example, has unsteady blade forces which repeat every revolution; in this case λ takes integer values k (k=1,2, etc). For a single blade, Fourier analysis of (13) gives

$$\bar{P} = (\bar{T}/2\pi a)\, e^{-i(k+m)\phi_1'};\ \omega = (k+m)\Omega \quad (m \text{ any integer}). \qquad (15)$$

Summation of this result for B identical blades equally spaced around the rotor leads to a resultant amplitude

$$\bar{P} = (B\bar{T}/2\pi a)\, e^{-i(k+m)\phi_1'} \quad (k+m = 0, \pm B \text{ etc}); \qquad (16)$$

here all harmonics (k+m) which are not multiples of B cancel because of the symmetry of the blading arrangement.

Blade forces which do not repeat every rotor revolution correspond to non-integer values of λ. The same theory applies as before, but the radiated frequencies $(\lambda+m)\Omega$ are no longer integral multiples of the rotation frequency Ω. As a result, the cancellation of harmonics referred to above no longer occurs.

In practice such non-repetitive blade forces usually have a continuous power spectrum, and it is necessary to convert the above results into power spectral form. The radiation spectrum of a single point force T, for example, follows form (12) and (14) as

$$G_p(\omega) = \left(\frac{\omega \cos\theta}{4\pi cR}\right)^2 \sum_{m=-\infty}^{\infty} J_m^2 \, G_T\left(|\omega - m\Omega|\right) . \qquad (17)$$

The generalization to include other force components is straightforward. Equation (17) was derived by Ffowcs Williams and Hawkings [6].

An alternative power spectral relation, for a single point force in subsonic circular motion, was developed by Morfey and Tanna [15] from Lowson's time-domain result [16]. The force is assumed to have components (T, D, 0) related by $(dD/dt)/(dT/dt) = \varepsilon = \text{const.}$, with a smooth power spectral density $G_T(\omega)$. The analysis assumes $(\Omega/\omega)^2 \ll 1$. Under these conditions,

$$G_p(\omega) \doteq \left(\frac{\omega}{4\pi cR}\right)^2 \{(\cos^2\theta + \tfrac{1}{2}\varepsilon^2\sin^2\theta)G_T(\omega) + \varepsilon M_{rot}\sin^2\theta \cos\theta \cdot \omega G_T'(\omega)$$
$$+ \tfrac{1}{4}\varepsilon^2\sin^2\theta \cdot \Omega^2 G_T''(\omega)\} ; \qquad (18)$$

terms of higher order in the rotational Mach number M_{rot} have been omitted, but are given up to M_{rot}^4 in [15].

Equation (18) has the advantage over the exact result (17) that the effects of force motion on the radiation spectrum are displayed explicitly. At low Mach numbers ($M_{rot}^2 \ll 1$), for example, the sound power spectrum is the same as for a stationary point force apart from an $(\Omega/\omega)^2$ term; thus there is no need to include source motion effects in estimating the broadband sound power from lower-speed fan blades [17;18] where both M_{rot}^2 and $(\Omega/\omega)^2$ are negligible. However, if $(\Omega/\omega)^2$ is not small, equation (18) breaks down and (17) must be used.

3.3 Effects of axial flow

A rotor placed in a uniform axial flow is equivalent to a rotor moving axially through a stationary fluid, apart from a uniform translation. For free-field radiation calculations, the stationary fluid/moving rotor description is simpler, since the sound field of any uniformly moving source is related to that of an equivalent stationary source by a Doppler transformation [19].

To first order in the axial Mach number M_x, the power radiated from a given equivalent source distribution is unaffected by the axial flow; but the separate amounts radiated upstream and downstream relative to the rotor are altered. For example, if the rotor is represented by a rotating array of uncorrelated point forces, each force having a broadband power spectrum proportional to ω^{-2} and a direction perpendicular to the relative mean flow, the sound power spectrum contains a Mach number correction factor

$$1 \pm \tfrac{3}{2} \cos^2\beta \cdot M_x \quad (\beta = \tan^{-1} M_{rot}/M_x \; ; \; M_R^2 \ll 1) \; . \qquad (19)$$

The ± signs in (18) refer to the sound power radiated on the ±x sides of the rotor; thus more sound power is radiated downstream, in this case, than upstream.

The point-force result (19) was obtained from (18) after applying the Doppler transformation mentioned above. It is interesting to note that a very similar result follows from the two-dimensional line-force model which is described in the next section.

4. DUCTED SOURCE MODELS (TWO-DIMENSIONAL)

A more appropriate acoustic model for ducted flow machines is a uniform hard-walled duct, containing a uniform steady flow on which the acoustic excitation is superimposed. The duct section may be circular or annular. If the duct is terminated on either side of the source with a known acoustic admittance, the wave equation (5) can be solved for any source distribution; details are given in [20].

In practice the usual termination is an open end, which leads to little reflection of propagating modes (except near cut-off) provided the smallest opening dimension exceeds $\frac{1}{4}\lambda$ [21]. Lining the duct with sound-absorbent material also tends to reduce the amplitude of waves reflected

back to the source. Under these conditions, the power radiated from the source, and the sound pressure inside the duct, may be estimated as if the duct were infinite.

Further analytical simplification may be achieved by using a two-dimensional model rather than an axisymmetric one. A two-dimensional acoustic model is particularly convenient since it means that the blade rows in the machine are represented by cascades. The larger the hub-tip ratio of the machine, the smaller is the influence of the duct curvature on the internal sound field. Even at small hub-tip ratios, however, a two-dimensional calculation of the sound field at each radius is expected to give reasonable estimates for the total sound power.†

Some results based on a two-dimensional infinite-duct model are given below, to illustrate the main features of sound generation in ducts with flow. Specific applications of these results are made in Section 5.

4.1 Radiation from two-dimensional source distributions

A single-frequency travelling-wave source distribution in the plane $x=0$ is specified by

$$S = \mathrm{Re}\ \bar{S}\, e^{i(\kappa y - \omega t)} \qquad (20)$$

Equation (20) represents a source pattern travelling at phase speed ω/κ in the tangential (y) direction. S is the area source density; thus the volume density q is $S\delta(x)$.

If this source distribution is superimposed on a uniform mean flow in the axial direction, the resulting sound field (assuming no reflections) is given by [20] as

---

† This will not be so if the source distribution varies radially on a scale small compared with both the blade span (h) and wavelength (λ). It is then necessary to "filter out" the high-wavenumber source components (for example, by defining a radial correlation length) before proceeding.

$$\bar{p} = e^{i(k_x^{\pm} x + \kappa y)} \frac{i}{2\alpha k} \bar{S} \qquad (x \gtrless 0) \quad , \tag{21}$$

where

$$\alpha = \{1 - \frac{(\kappa/k)^2}{1-M_x^2}\}^{\frac{1}{2}} \qquad (k = \omega/c)$$

and

$$\frac{k_x^{\pm}}{k} = \frac{\pm\alpha - M_x}{1-M_x^2}$$

The corresponding intensity on either side of the source follows from

$$I_{\pm} = \frac{1}{2} |\bar{p}|^2 \frac{\alpha}{\rho c} (\frac{1 - M_x^2}{1 \mp \alpha M_x})^2 \qquad (x \gtrless 0;\ \alpha \text{ real}). \tag{22}$$

If the source phase speed is subsonic, α becomes imaginary and the intensity is zero. This corresponds to cut-off in an axisymmetric duct.

The sound field of higher-order source distributions may be found from (21) by differentiation. Of particular interest in connection with blade noise is the result for a two-dimensional force distribution, with axial and tangential components given by

$$(X, Y) = \mathrm{Re}(\bar{X}, \bar{Y})\, e^{i(\kappa y - \omega t)} \tag{23}$$

per unit area of the source plane. In this case the pressure amplitude is different on the two sides;

$$\bar{p} = e^{i(k_x^{\pm} x + \kappa y)} \frac{1}{2\alpha} \{(\frac{k_x^{\pm}}{k}) \bar{X} + (\frac{\kappa}{k}) \bar{Y}\} . \tag{24}$$

Equations (21), (22) and (24) are restricted to mean flows in the axial direction. They may be modified to allow for a tangential flow component, with Mach number M_y, by interpreting the frequency ω and wavenumber k as values relative to the tangential flow. Thus if ω_o is the actual fixed-frame frequency, we have

$$\omega = \omega_o - \kappa c M_y \tag{25}$$

The pressure field is then given directly by (21) or (24), while the intensity expression (22) is multiplied by (ω_o/ω) to give the axial intensity in fixed coordinates [20].

4.2 Phased array of line forces

Where the blade chord is small compared with the acoustic wavelengths of interest, the unsteady loading on each blade is acoustically equivalent to a single line force. A radially-aligned blade, for example, which applies an axial force F per unit span to the fluid, is approximately represented by a force distribution

$$X = F\delta(y-y_1) \tag{26}$$

where y_1 is the position of the blade in the two-dimensional model.

Summation of (26) over all the blades in a rotor or stator row, followed by Fourier analysis into travelling-wave components as in (23), proceeds in the same way for the point-force description. If the blades are identical and equally spaced, the following results are obtained for a travelling-wave modulation of the blade forces.

(a) For a rotor with blade spacing d_R, modulated by a disturbance of the form $\cos k_w y$, the axial force distribution is confined to blade-passing harmonics given by

$$\bar{X} = \frac{\bar{F}}{d_R} e^{\mp ik_p y_1} \quad \left(\text{force on each blade} = \mathrm{Re}\ \bar{F} e^{-ik_w y_1}\right) \tag{27}$$

with $\kappa = \pm k_p - k_w$ and $\omega = \pm k_p u_{rot}$.† Here $k_p = 2\pi p/d_R$, and p (=1,2, etc) is the blade-passing harmonic order.

(b) For a stator with blade spacing d_S, modulated by a disturbance of the form $\cos k_w(y - u_{rot}t)$, the axial force distribution is given by

$$\bar{X} = \frac{\bar{F}}{d_S} e^{\mp ik_s y_1} \quad \left(\text{force on each blade} = \mathrm{Re}\ \bar{F} e^{ik_w(y-u_{rot}t)}\right) \tag{28}$$

with $\kappa = k_w \pm k_s$ and $\omega = k_w u_{rot}$. Here $k_s = 2\pi s/d_S$ and s is any positive integer.

Stator-rotor interaction is a special case of (27) in which $k_w = k_s$; likewise rotor-stator interaction is described by (28) with $k_w = k_p$. In each case the resulting force distribution has $\kappa = (k_p \pm k_s)\mathrm{sgn}\ \omega$, corresponding to a circumferential mode number $m = pB \pm sV$ as given by Tyler and Sofrin [22].

---

† For subsonic rotors, the lower signs ($\omega < 0$) correspond to non-propagating waves.

4.3 Uncorrelated array of broadband line forces

The single-frequency results (24), (27), (28) may also be applied in power spectral form to describe the radiation from nonperiodic blade forces. For example, the intensity spectrum radiated from an array of uncorrelated lift forces L(t) per unit span is [23]

$$\left(\frac{dI}{d\omega_o}\right)_{\pm} = \frac{1}{16}\,\frac{\omega_o G_L(\omega_o)}{\rho c^2 d}\,A_{\pm} \qquad (\omega_o = \text{fixed-frame frequency}). \tag{29}$$

The factor $A_{\pm}$ in (29) accounts for mean flow in both the x and y directions; it depends on the angle β of the relative flow. To first order in Mach number,

$$A_{\pm} \doteq 1 \pm M_x \cdot \frac{8}{3\pi}\cos^2\beta \cdot \left(1 - \frac{M_{rot}}{M_x}\, g \tan\beta\right), \quad \left(\beta = \tan^{-1}\frac{M_{rot}-M_y}{M_x}\right) \tag{30}$$

where $g = 2 + (\omega/G_L)(dG_L/d\omega)$ is determined by the slope of the lift spectrum. The term involving g arises from the Doppler frequency shift encountered with moving blades ($M_{rot} \neq 0$).

The special case $g=0$ (lift spectrum proportional to ω^{-2}) gives $A_{\pm} = 1 \pm M_x \cdot \frac{8}{3\pi}\cos^2\beta$, as compared with $1 \pm M_x \cdot \frac{3}{4}\cos^2\beta$ for the point-force unducted rotor model (equation 19). Equation (30) is compared with fan noise measurements in Section 7.

5. ESTIMATES OF BLADE-PASSING SOUND IN AXIAL FLOW MACHINES

Estimates are given in this section for the blade-passing sound field of an isolated rotor, and of rotor-stator and stator-rotor combinations. These are all based on the acoustic analogy of Section 2, together with the two-dimensional acoustic model of Section 4. Results are also quoted for the transmission of sound through a row of blades, calculated by Amiet [24] on the same basis.

All the results which follow are strictly limited to blade chords small compared with the sound wavelength. Calculations in which the restriction $\ell \ll \lambda$ is removed are described in Section 6.

5.1 Isolated rotor in sinusoidal velocity wake ($M_R^2 \ll 1$)

At low Mach numbers, the main source of propagating waves (i.e. $|\kappa| < k$) is the unsteady lift experienced by the rotor blades as they pass through the wake pattern. Propagation of the pth blade-passing harmonic requires $|k_p - k_w| < k_p M_{rot}$ (equations (21), (27)); so at low Mach numbers no energy is radiated unless $k_w \doteq k_p$.

The nonuniform velocity entering the rotor is defined by

$$v_x = v_{x0} \cos k_w y \; ; \quad (v_{x0}/u_{rot}) = a_w \; , \tag{31}$$

and is superimposed on a uniform axial flow. The fluctuating axial force component due to each blade may be estimated from incompressible isolated-airfoil theory [25-27], provided the gap between adjacent blades is large compared with the gust wavelength along the blade. This gives

$$\bar{F} \doteq \pi \ell_R \rho \, V_R \left(\bar{v}_n + \frac{C_{LR}}{\pi} \bar{v}_s\right) K_L \sin \beta_1, \quad (\sin 2\beta_1 \gg 1/\pi p) \tag{32}$$

where the fluctuating velocity amplitudes normal and parallel to the blade are

$$\bar{v}_n \doteq -v_{x0} \sin \beta_1 \; , \quad \bar{v}_s \doteq v_{x0} \cos \beta_1 \; . \tag{33}$$

Equations (32) and (33) take no account of blade camber, and the effective flat-plate stagger angle is taken as the inlet relative flow angle β_1.

At high reduced frequencies (gust wavelength along blade $\ll 5\ell_R$) the lift response function K_L may be replaced by its asymptotic form. The following simple expression for the sound field far from the rotor plane (x=0) is then obtained using equation (24).

$$\frac{|\bar{p}_p|}{\rho u_{rot}^2 a_w} \doteq \frac{1}{2a}\left(\frac{\sigma_R}{2p}\right)^{\frac{1}{2}} \sin^{\frac{1}{2}}\beta_1 \cdot \left|(1 - \frac{C_L R}{\pi}\cot\beta_1)(1 \pm \frac{k_p - k_w}{k}\cot\beta_1)\right|, \quad (x \gtrless 0) \qquad (34)$$

equation (34) is valid for $\sin 2\beta_1 \gg 1/\pi p$, $\sigma_R \sin\beta_1 \gg 0.05/p$ and real values of a.

This result is compared with measurements in Section 7.2. Although it implies that the radiated power becomes infinite as cut-off is approached from above (i.e. $a \to 0$), Whitehead [28] and Mani [29] have shown that the incompressible lift calculation breaks down in the cut-off region. The fluctuating lift in fact tends to zero, and the sound power to a finite limit, at cut-off [28].

5.2 Isolated rotor in sinusoidal temperature wake ($M_R^2 \ll 1$)

According to Section 2, entropy perturbations incident on a rotor combine with the blade-to-blade potential flow field to produce an equivalent acoustic source distribution. At low Mach numbers the dominant source term may be written

$$q = (\rho/C_p)\, v_i v_j \frac{\partial^2 s'}{\partial x_i\, \partial x_j} \quad ; \qquad (35)$$

the working fluid is assumed to be a perfect gas with constant γ.

A sinusoidal temperature distortion (at constant pressure) is defined by

$$\frac{T'}{T} = \frac{s'}{C_p} = a_t \cos k_t y \quad , \qquad (36)$$

and is superimposed on the otherwise uniform mean flow entering the rotor. Because of the low Mach number restriction, sound waves excited at p times blade-passing frequency will propagate only if $k_t \doteq k_p$.

If the axial variation of s' is neglected, only the tangential velocity perturbations v_y contribute to the source term (35). Linearized theory for a low-solidity rotor at low relative Mach numbers gives, due to lift forces,

$$v_y \doteq \pm\tfrac{1}{4}\,\sigma_R\,V_R\,C_{LR}\,\{1 + 2\sum_{p=1}\cos k_p(y - y_1)\,e^{\mp k_p x}\}\quad,\ (x \gtrless 0)\ ; \tag{37}$$

there are also contributions from blade thickness and drag, but these will be neglected. It is important to note that equation (37) is restricted to low-order harmonics ($p \lesssim 1/\sigma_R$); higher-harmonic amplitudes are overestimated by the low-solidity model.

The acoustic source strength is proportional to v_y^2, which may be written as

$$v_y^2 = \tfrac{1}{16}\,(\sigma_R V_R C_{LR})^2\,\{1 + 4e^{\mp k_1 x}\cos k_1(y-y_1) + (\text{higher-order interactions})\} \tag{38}$$

The second term alone in (38) is used below to estimate the propagating sound field at blade-passing frequency (p=1). Products of higher-order harmonics such as (1,2), (2,3) etc. will also contribute to the source moment $S = \int q\,dx$ at this frequency, in the ratio $\frac{1}{3}$, $\frac{1}{5}$ etc according to (37); however, their true contributions will be lower in practice than the low-solidity model indicates, and may be neglected without much error for σ_R values in the range 0.4–1.

The estimated pressure amplitude, for waves propagating on either side of the rotor, follows from (21) as

$$\frac{|\bar{p}_1|}{\rho V_R^2 a_t} \doteq \frac{\sigma_R^2 C_{LR}^2}{8 a M_{rot}} \quad (a_{real}\ ;\ 0.4 < \sigma_R < 1)\ . \tag{39}$$

5.3 Isolated rotor: scattering of potential field by inflow distortions

If the restriction to low Mach numbers is removed from case (5.1), it no longer follows that blade lift fluctuations are the main source of blade-passing sound. Scattering of the rotor potential field by a nonuniform inlet flow was recognised by Ffowcs Williams and Hawkings [6] as a source of sound at high subsonic speeds, the relevant acoustic source term being

$$q = \rho_o \frac{\partial^2 v_i v_j}{\partial x_i \partial x_j} \qquad (40)$$

The blade passing sound field produced by this mechanism has been calculated for a low-solidity rotor [30], using a compressible linearized estimate of the rotor potential field. If the wake distortion wavelength is equal to the blade spacing, the result is simply

$$\frac{|\bar{p}_1|}{a_w \Delta p} \doteq \frac{M_{rot}}{1 \pm M_x}\left(1 - \frac{M_{rot}^2}{1 \pm M_x}\right) \qquad (x \gtrless 0) \quad ; \qquad (41)$$

equation (41) is valid for $\sigma_R^2 << (1 - M_x^2)$. As in the previous calculation, only the blade lift component of the rotor field is included; Δp is the corresponding mean pressure rise across the rotor.

Comparison of (34) and (41) suggests that if the rotor loading coefficient $\Delta p/\rho u_{rot}^2$ exceeds about 1, the quadrupole scattering mechanism may well predominate at Mach numbers as low as $M_R = 0.5$, especially on the upstream side of the rotor.

5.4 Transmission of sound through an isolated blade row

The same two-dimensional blade-row model with $\ell << \lambda$ has been used by Amiet [24], to estimate the reflection and transmission coefficients of a blade row for incident sound waves. A typical situation is sketched in Figure 2. The long-wavelength assumption implies that the flow through the cascade is quasi-steady locally; thus the unsteady lift on each blade is given by the steady-flow cascade relations, to good accuracy provided $\ell/\lambda << 1-M$. The scattered sound field then follows from the unsteady forces, using the acoustic analogy.

Among the results obtained is the following equation for transmission upstream through a stationary cascade of flat plates:

$$\frac{|\bar{p}_{tr}|}{|\bar{p}_{inc}|} = \frac{\cos \phi_{inc} - M_x}{\cos \phi_{inc} - M_x + F} \quad , \qquad (42)$$

where for high-solidity cascades

$$F \doteq \frac{M(1 - M_x^2)}{2(1 - M^2)} \quad \frac{\sin^2(\phi_{inc} + \xi)}{\cos \xi} , \quad [\sigma^2 >> 0.2(1 - M_x^2)] . \qquad (43)$$

Equation (42) predicts zero transmission when $\cos \phi_{inc} = M_x$, which corresponds to cut-off of the incident wave. 100% transmission is predicted for zero flow (M=0) and for waves travelling parallel to the blades ($\phi_{inc} = -\xi$). There is no dependence on frequency for a given incidence angle, although ϕ_{inc} varies with frequency for a given mode.

Amiet has compared his results with numerical calculations [31] based on the same physical model (i.e. two-dimensional flat-plate cascade at zero incidence), and finds good agreement over the whole range $\ell/\lambda < 1-M$. It is interesting to note, in passing, the conceptual similarity between Amiet's matching procedure and that used by Whitehead to describe the vibration of cascade blades in an incompressible flow [32].

5.5 Rotor-stator interaction (M_R^2, $M_S^2 << 1$)

In low Mach number fans and compressors, rotor-stator interaction tones are generated mainly by fluctuating blade forces [8]. On the upstream blade row, periodic forces arise from the potential field of the downstream blades; their magnitude, and hence the radiated power, falls off rapidly as the axial gap between the blade rows is increased. The downstream blade row, on the other hand, cuts through the wakes of the upstream blades; and if the upstream row has a solidity of order 1 or more, its downstream potential field is generally negligible by comparison.

The sound intensity radiated either side of a rotor-stator combination is estimated in [8] as follows, for a single propagating mode well above cut-off.

(a) Rotor lift fluctuations due to stator potential velocity field:

$$\frac{I_p}{\rho c^3} \doteq \frac{K_p}{32\pi^2 p} \cdot \left(\frac{V}{pB}\right) \sigma_R \sigma_S \, C_{LS}^2 \, M_S^4 \sin^2\beta_2 , \qquad (44)$$

where $K_p = e^{-2k_p \bar{x}}$ allows for the axial decay of the potential field. Equation (44) requires that $\exp 2\pi p\sigma_s >> 1$ (high-solidity approximation to potential field), and the rotor lift fluctuations are based on the Kemp-Sears isolated airfoil theory [33] for high reduced frequencies (i.e. $n_R >> 1/2\pi$).

The corresponding result for a stator-rotor combination is obtained by interchanging α and β, and also subscripts R, S; K_p remains unaltered. Note that the flow angles are given their values on the side nearer the interacting blade row.

(b) Stator lift fluctuations due to rotor wakes:

$$\frac{I_p}{\rho c^3} \doteq \frac{K_w}{16}\left(\frac{V}{pB}\right)\pi_R^2\sigma_S\left(M_R^2 M_S^3/M_{rot}\right)\left[1-\frac{C_{LS}}{\pi}\cot(\beta_2+\alpha_1)\right]^2 \sin^2(\beta_2+\alpha_1).s \qquad (45)$$

where $K_w = (\delta^*/\tfrac{1}{2}C_D\ell)_R^2$ is a wake shape parameter based on the displacement thickness at entry to the stator.† Equation (45) is subject to the restriction that the rotor wakes remain distinct; this requires

$$(\bar{x}/\ell_R)^{\frac{1}{2}} \ll \frac{1}{2p}\cos^{3/2}\beta_2.\left(d/C_D^{\frac{1}{2}}\ell\right)_R . \qquad (46)$$

Again, the lift fluctuations are based on high-frequency isolated airfoil theory, which implies $n_S \gg (1/2\pi,\ \sigma_S/2\cos\alpha_1)$.

The corresponding result for a stator-rotor combination is obtained by the same substitutions as in (a); in addition, the factor (V/pB) becomes 1/p.

Equations (44) and (45) are compared with measurements in Section 7.3. Note that the results quoted above refer to a single interaction mode m = pB - s so the total intensity at p × blade-passing frequency is the sum of the intensities I_p predicted for each mode above cut-off.

† For an estimate of K_w, see equation (47) below.

6. TWO-DIMENSIONAL CASCADE MODELS WITH $\ell \ll \lambda$

The acoustic analogy used to obtain the previous results runs into practical difficulties when the blade chord is not small compared with the sound wavelengths of interest. The back-reaction of the sound field on the equivalent acoustic source distribution becomes significant, and in order to find the source distribution it is necessary to know the sound field.

Some progress has been made recently in dealing with this situation, and two types of problem can now be solved analytically or numerically. These are :

(a) Interaction of sound waves with non-lifting flat-plate cascades in compressible flow. Here a linearized analysis is adequate, and the basic flow is uniform. Outside the blade wakes, the velocity perturbations are irrotational.

(b) Vorticity perturbations incident on a cascade as in (a). The incident vorticity field is unaffected to first order by the blades, except that vorticity is shed from the trailing edges. Thus the boundary conditions on the pressure field over the blade surfaces are that the associated normal velocity perturbation should cancel that due to the incident vorticity, and that the pressure jump should not be infinite across the trailing edge.

The analyses available to date are described briefly below.

6.1 Sound transmission through blade rows

The simplest model in which there is no restriction on ℓ/λ is the semi-actuator disk model of Kaji and Okazaki [34], in which the blade spacing tends to zero. Their results for $\ell/\lambda \ll 1$ agree well with the high-solidity limit of Amiet's theory [24], as expected. The model represents the flow perturbations within the blade passages by plane acoustic waves; these are then matched across the leading-edge and trailing-edge planes to the perturbations outside.

An alternative model which also allows analytical solutions has been used by Mani and Horvay [35]. No restriction is placed on the blade spacing in their model; but in matching the interior and exterior wave solutions the leading and trailing edges of the cascade, the blades are regarded as infinite. Remarkably close agreement is obtained with available numerical solutions.

Kaji and Okazaki [31], Whitehead [28] and Smith [36] have developed computer programmes for numerical solution of the linearized perturbation equations, and some results are given in [31] for transmission and reflection of sound waves incident from downstream on a flat-plate cascade. None of the theoretical predictions, however, has been checked experimentally.

6.2 Sound scattered by vorticity incident on blades

The numerical methods mentioned above will also predict the sound field radiated upstream and downstream when spanwise vorticity perturbations are convected through the cascade. Mention has already been made of Whitehead's calculations [28], which show significant departures from the simple theory of Section 5.1 close to cut-off, even though the ℓ/λ value used was only about 0.05. No results are available for ℓ/λ values of order 1 or more, where the simple theory breaks down completely.

An analytical solution for scattering by an isolated flat-plate airfoil at zero mean incidence has been worked out by Adamczyk and Brand [37]; like the numerical solutions for flat-plate cascades, their result may be applied to either incident sound or vorticity perturbations. In contrast to the cascade solutions at present available, the incident disturbance is allowed to vary in the spanwise direction.

Unfortunately, no experimental confirmation is yet available for the vorticity scattering theories in the ℓ/λ range above one, where their predictions diverge from Section 5.1.

7. COMPARISONS BETWEEN THEORY AND EXPERIMENT

The theoretical results reviewed above fall into three categories:

1. Predictions of the sound radiated from specified acoustic source distributions, in the presence of uniform flow;
2. Predictions of sound radiated from an isolated blade row operating in a specified non-uniform flow;
3. Predictions of rotor-stator interaction tones from steady-flow aerodynamic data.

In this section, predictions from each category are compared with experimental d

7.1 Mean flow effect on fluctuating-lift radiation

The two-dimensional theory of Section 4 predicts a difference, due to mean flow, between the power radiated upstream and downstream by an array of fluctuating lift forces. Lipstein and Mani [38] have confirmed this effect using a ducted rotor of hub-tip ratio 0.74, operating in the wakes of a regular array of rods. The blade-passing sound power was measured on the inlet and exhaust sides, and for a particular configuration (Figures 15 and 16 of [38]) differences of up to 9 dB were measured over the Mach number range M_R=0.32-0.53. In this range only one interaction mode was able to propagate in either direction, and the predicted power differences followed the measurements within 1 dB except very close to cut-off.

Further indications of the same effect occur in some broadband fan noise measurements reported by Snow [39]. The fan consisted of an IGV/rotor/OGV combination of 0.55 hub-tip ratio. Here the source is less well defined, but is assumed to consist of fluctuating lift forces on the blades, with no correlation between blades. Equation (30) then predicts the exhaust/inlet power ratio in a narrow frequency band, assuming multi-mode propagation ($kr_t \gg 1$). The power ratio was measured in 100 Hz bands, at frequencies chosen to avoid blade-passing harmonics; measured and predicted values are compared in Figure 3.

At each frequency two theoretical curves are shown, one for the stationary blades (IGV, OGV) and one for the rotor. The rotor prediction involves the spectrum slope parameter g, which was estimated from the spectrum of the total (inlet + exhaust) power by means of equation (29). In general the measured data lie between the rotor and stator predictions.

Measurements were also made at lower frequencies, but these show little significant difference between exhaust and inlet radiated power.

7.2 Isolated blade row in a measured non-uniform flow

Two types of inflow disturbance are discussed under this heading: (a) turbulence, and (b) periodic wakes.

(a) Rotor in turbulent flow:

Following the early work of Sharland [17], who measured the power radiated by a rotor running in turbulence of known intensity but unknown scale, some more detailed measurements have recently been reported by Chandrashekhara [40].

An open fan rotor was run over a range of speeds (M_{tip} = 0.08 to 0.28) with a turbulence-generating ring upstream of the blades. Measurements of the fixed-coordinate turbulence spectrum showed most of the energy to be at low frequencies compared with the fan rotation rate, leading to a sound power spectrum concentrated around multiples of the blade-passing frequency.

By inserting scale and intensity measurements into an expression for the fluctuating lift, and then treating the rotor as an array of point forces, the sound power around blade-passing frequency was estimated at each speed; the maximum h/λ value was 0.22. Reasonable agreement was found between the predicted and measured power, the prediction falling about 5 dB low on average.

(b) Blade row passing through periodic wakes:

Smith [36] has measured the blade-passing sound field downstream of a ducted rotor of hub-tip ratio 0.75, running at low Mach numbers (M_{rot} < 0.1) with a sinusoidal distortion imposed on the inlet flow. The distortion pattern consisted of 24 cycles around the annulus, and the rotor had 23 blades; cut-off of the m = -1 wave is therefore expected at $M_{rot} \doteq 0.0$

Introducing the flow distortion led to an appreciable increase in the blade-passing pressure amplitude above the cut-off speed, by a factor of 4 or more. The measured amplitudes are plotted in Figure 4, showing a pronounced rise as cut-off is approached. The three sets of measurements correspond to three different rotor incidence angles, ranging from zero to -18 degrees; the blade camber was 20 degrees.

On the normalized scale chosen for Figure 4, the simplified theory of Section 5.1 predicts very nearly equal amplitudes for each of the three incidence values at speeds well above cut-off. The measurements unfortunatel do not extend much beyond cut-off; but the three incidence angles collapse quite closely, and appear to be approaching the predicted value at the upper end of the speed range.

Peirce [41] has measured the blade-passing sound field radiated fro the inlet of a low speed ducted rotor (M_{rot} = 0.09 - 0.16), with an equal num of stator blades placed at four different positions downstream ($\bar{x}/\ell_R$ = 0.3-1.

The wake pattern of the rotor had previously been measured by P.D. Yardley at Southampton, using a stationary hot-wire probe and a time-sampling technique, and was harmonically analysed to extract the blade-passing component. Mid-span values were then inserted into the two-dimensional theory of Section 5.1, and the on-axis SPL predicted neglecting reflections from the duct inlet and exhaust.†

Measured and predicted levels are compared in Table I, for the two closest stator positions. The agreement is good; but at the largest separation the predicted levels are 5-10 dB high. A possible reason is that the rotor wakes become skewed as they travel downstream, so partial cancellation occurs along the stator span.

7.3 Interaction tone predictions from steady-flow aerodynamic data

Lipstein and Mani [38] predicted the blade-passing sound power in their experiment already referred to, by estimating the rotor blade forces according to incompressible theory and then using a two-dimensional acoustic model as in Section 4 [42]. Figure 5, based on Figure 16 of [38], shows results obtained for the exhaust-radiated power.

The predicted curve in Figure 5 has been modified from the original, using an improved correlation for wake displacement thickness [43]:

$$\frac{\delta^*}{\frac{1}{2}C_D\ell} \simeq 1 + \exp - \left(\frac{0.11\ x'}{C_D\ell}\right) \qquad (47)$$

The empirical correction (-3.5 dB) introduced by Lipstein and Mani in their fluctuating-lift-estimates has been removed, although a correction of this order would probably result from the chordwise-velocity term, which was omitted from the lift calculation in [38].

The agreement in Figure 5 is nevertheless quite good over the speed range above cut-off for the lowest interaction mode. The corresponding h/λ range is 0.3-1.1, so the neglect of reflected waves from the duct inlet and

† This would be appropriate for $kr_t \gg 1$; actual values ranged from 1.6 to 3. A more accurate radiation calculation would predict on-axis levels perhaps 1-2 dB higher than given.

exhaust is fairly well justified.

In Figures 6–8, measurements of inlet-radiated sound power from aircraft-engine fans and compressors are compared with the low Mach number estimates of section 5.5. The machines are all multistage, and the results plotted are for the first-rotor blade-passing frequency. The predicted curves are estimates for the sound power due to lift fluctuations on the first two blade rows only (i.e. IGV and first rotor). Throughout the speed range for which results are given, each pair of interacting blade rows produced no more than one propagating mode, so the single-mode predictions of Section 5.5 were used without alteration.

The wake interaction curves in Figures 6–8 are based on equation (47), whth an assumed IGV loss coefficient of 0.05. For engines A, C_1 and D this mechanism accounts for most of the predicted power output, and the measured levels are mostly within 6 dB. There is a tendency for the measured levels to fall below the predictions at the higher Mach numbers, which may be due to blockage by the inlet guide vanes.

For engine C_2 in Figure 7, the IGV-rotor interaction is cut off over the whole speed range, but the rotor-stator interaction is still able to radiate. The sound power prediction for this interaction is uncertain, as it involves the stator lift coefficient which was not known; assuming a value in the range 0.7–1.0 (as for the upstream rotor) gives the broken line in Figure 7, which is about 10 dB too high.

8. SUMMARY AND CONCLUSIONS

(a) Lighthill's acoustic analogy, with appropriate modifications, leads to a number of useful predictions concerning axial flow machinery noise. In particular, equivalent acoustic sources are identified in section 2 for blades operating in non-uniform flows.

(b) A major attraction of the acoustic analogy is that simple analytical results are available for radiation from sources in a uniform flow, either without boundaries as in section 3, or inside a uniform hard-walled duct as in section 4.

(c) A summary is given in section 5 of results, based on the acoustic analogy, for blade passing radiation from ducted rotors.

(d) For acoustic wavelengths shorter than the blade chord, the processes of sound generation and scattering by blade rows are interlinked, and the acoustic analogy is no longer appropriate. More elaborate methods of calculation are then necessary, as outlined in section 6.

(e) There is very little experimental evidence against which the various theories may be tested. Such evidence as exists is discussed in section 7. The acoustic analogy predictions are borne out within the uncertainty of the measurements (acoustic and aerodynamic), except where waves are excited close to cut-off.

(f) It would be useful to know the limitations of the acoustic analogy approach in more detail. The numerical solutions described in section 6 have already been compared with the acoustic analogy approximation for sound transmission through blade rows; further comparisons are required for the sound scattered from incident vorticity perturbations.

(g) Application of even the acoustic analogy to turbomachinery noise calculations is held up by ignorance of the unsteady flow around blades, particularly in the tip and hub regions. Further experimental work is required to complement the theoretical studies reviewed in this paper.

REFERENCES

1. L. GUTIN 1936 Phys.Z.SowjUn. 9, 57-71. Translated as NACA TM 1195 (194
2. L. GUTIN 1942 Zhur.tekh.phys. 12, 76.
3. M.J. LIGHTHILL 1952 Proc.Roy.Soc.(London) A 211, 564-587
4. N. CURLE 1955 Proc.Roy.Soc.(London) A 231, 505-514
5. S.L. BRAGG and R. BRIDGE 1964 J.Roy.Aero.Soc. 68, 1-10
6. J.E. FFOWCS WILLIAMS and D.L. HAWKINGS 1969 J.Sound Vib. 10, 10-21
7. C.L. MORFEY 1969 in Aerodynamic Noise (Ed. H.S. Ribner), 299-329. Toronto University Press.
8. C.L. MORFEY 1970 J.Basic Eng.: Trans. ASME (Series D) 92, 450-458.
9. B.-T. CHU and L.S.G. KOVASZNAY 1958 J.Fluid Mech. 3, 494-514
10. P.J. WESTERVELT 1963 J.Acoust.Soc.Am. 35, 535-537.
11. P.J. WESTERVELT 1970 in Proceedings of 1969 ARL Symposium on Nonlinear Acoustics, University of Texas at Austin, 165-181.
12. T.F.W. EMBLETON and G.J. THIESSEN 1962 J.Acoust.Soc.Am. 34, 788-795.
13. S.E. WRIGHT 1969 J.Sound Vib. 9, 223-240.
14. M.V. LOWSON and J.B. OLLERHEAD 1969 J.Sound Vib. 9, 197-222
15. C.L. MORFEY and H.K. TANNA 1971 J.Sound Vib. 15, 325-351
16. M. V. LOWSON 1969 Proc.Roy.Soc.(London) A 286, 559-572
17. I.J. SHARLAND 1964 J.Sound Vib. 1, 302-322
18. B.D. MUGRIDGE 1971 J.Sound Vib. 16, 593-614
19. C.L. MORFEY 1972 ISVR Memorandum No.453, University of Southampton.
20. C.L. MORFEY 1971 J. Sound Vib. 14, 37-55
21. C.L. MORFEY 1969 J. Sound Vib. 9, 367-372
22. J.M. TYLER and T.G. SOFRIN 1962 S.A.E. Transactions 70, 309-332
23. C.L. MORFEY 1972 in Proceedings of 1970 Symposium on Fluid Mechanics and Design of Turbomachinery, Pennsylvania State University.

24. R. AMIET 1971 AIAA J. 9, 1893-1894.

25. W.R. SEARS 1941 J.Aero.Sci. 8, 104-108

26. J.H. HORLOCK 1968 J.Basic Eng.: Trans.ASME (Series D) 90, 494-500.

27. C.L. MORFEY 1970 " " " " " 92, 663-665.

28. D.S.WHITEHEAD 1970 CUED/A-Turbo/TR15, Dept. of Engineering, Univ. of Cambridge

29. R. MANI 1972 in Proceedings of 1970 Symposium on Fluid Mechanics and Design of Turbomachinery, Pennsylvania State University.

30. C.L. MORFEY 1971 J.Acoust.Soc.Am. 49, 1690-1692

31. S. KAJI and T. OKAZAKI 1970 J.Sound Vib. 11, 355-375

32. D.S. WHITEHEAD 1959 Proc.I.Mech.E. 173, 555-574

33. N.H. KEMP 1952 J.Aero.Sci. 19, 713-714

34. S. KAJI and T. OKAZAKI 1970 J.Sound Vib. 11, 339-353

35. R. MANI and G. HORVAY 1970 J.Sound Vib. 12, 59-83

36. S.N. SMITH 1971 CUED/A-Turbo/TR29, Dept. of Engineering, Univ. of Cambridge

37. J.J. ADAMCZYK and R.S. BRAND (submitted to J.Sound Vib. 1972)

38. N.J. LIPSTEIN and R. MANI 1970 J.Basic Eng.:Trans.ASME (Series D) 92, 155-164

39. R. SNOW 1970 M.Sc. Dissertation, ISVR, University of Southampton.

40. N. CHANDRASHEKHARA 1971 J.Sound Vib. 18, 533-543

41. I.R. PEIRCE 1972 M.Sc. Dissertation, ISVR, University of Southampton.

42. R. MANI 1970 J.Basic Eng.: Trans.ASME (Series D) 92, 37-43

43. B.D. MUGRIDGE and C.L. MORFEY 1972 J.Acoust.Soc.Am. (in press)

TABLE I

Measured and predicted blade-passing SPL on fan inlet axis, 2.4m from inlet

(rotor diameter 0.255 m)

Fan speed (rev/min)		1500	2000	2800
SPL (dB re $20\mu N/m^2$): $\bar{x}/\ell_R = 0.3$	measured	87	90	102.5
	predicted	85.0	91.5	99.7
SPL (dB re $20\mu N/m^2$): $\bar{x}/\ell_R = 0.55$	measured	80.5	87	98.5
	predicted	81.2	86.9	98.7

TABLE 2

Compressor/fan Data	Aircraft Engines				Single Stage Fans	
	A	C_1	C_2	D	[39]	[41]
IGV No. Solidity Stagger (degrees)	24 0.95 7	37 0.99 16	85 1.26 14	28 1.02 12	43 0.90 13	- -
Axial gap/IGV chord	0.30	0.67	0.88	0.30		-
1st rotor No. Solidity Stagger (degrees) (r_h/r_t) entry	23 1.23 38 0.36	31 0.79 35 0.56	31 0.79 35 0.56	29 1.19 28 0.50	31 0.90 32 0.55	14 0.66 66 0.50
Axial gap/rotor chord	0.21	0.26	0.32	0.27		variable
1st stator No. Solidity	50 1.70	38 0.87	38 0.87	28 1.07	50 1.74	14 0.75

ACKNOWLEDGEMENTS

Thanks are due to my former colleagues at Bristol Siddeley Engines and the Department of Aeronautics and Astronautics, Southampton University, to whom I owe my early education in acoustics; and to the various members of the Institute of Sound and Vibration Research with whom I have worked over the past four years, both staff and research students.

Figure Captions

Fig.1 Definition sketch for free-field radiation from ring source.

Fig.2 Plane-wave transmission through cascade.

Fig.3 Sound radiation from broadband lift forces on fan blades: flow convection effect.

Fig.4 In-duct measurements of rotor blade-passing pressure field: rotor in sinusoidally distorted flow.

Fig.5 Sound power at blade-passing frequency radiated from rotor exhaust, with and without upstream wakes.

Figs.6,7,8 Inlet-radiated sound power at blade-passing frequency of 1st rotor: comparison with low Mach number theory.

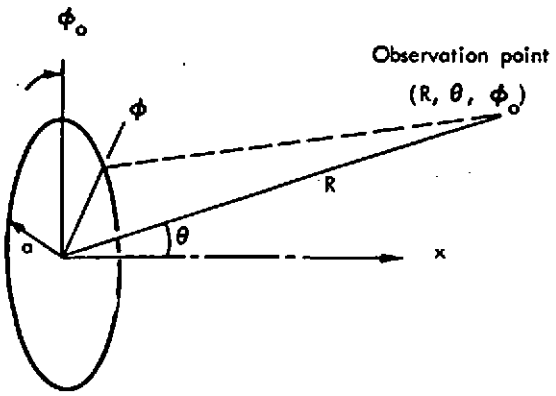
ϕ_o
Observation point
(R, θ, ϕ_o)
ϕ
R
a
θ
x

Fig. 1

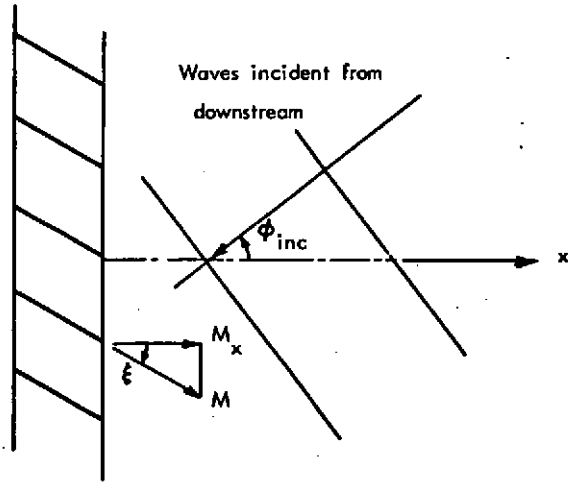
Waves incident from
downstream
ϕ_{inc}
x
M_x
ξ
M

Exhaust/inlet sound power ratio (100 Hz bandwidth)

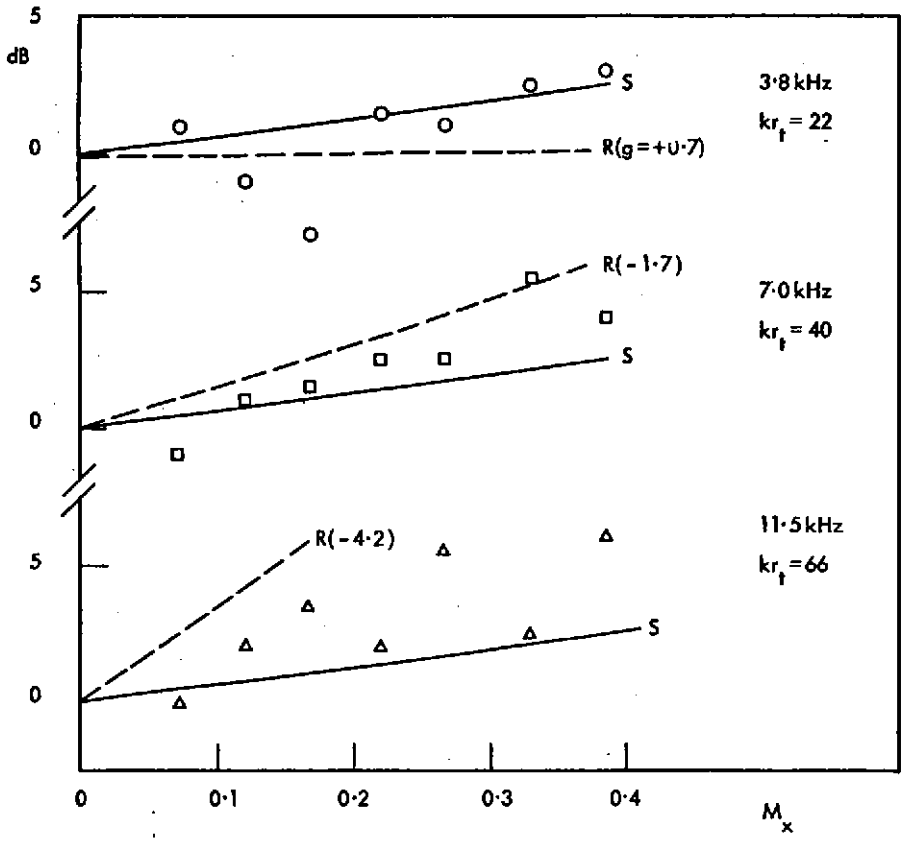

Fig. 3

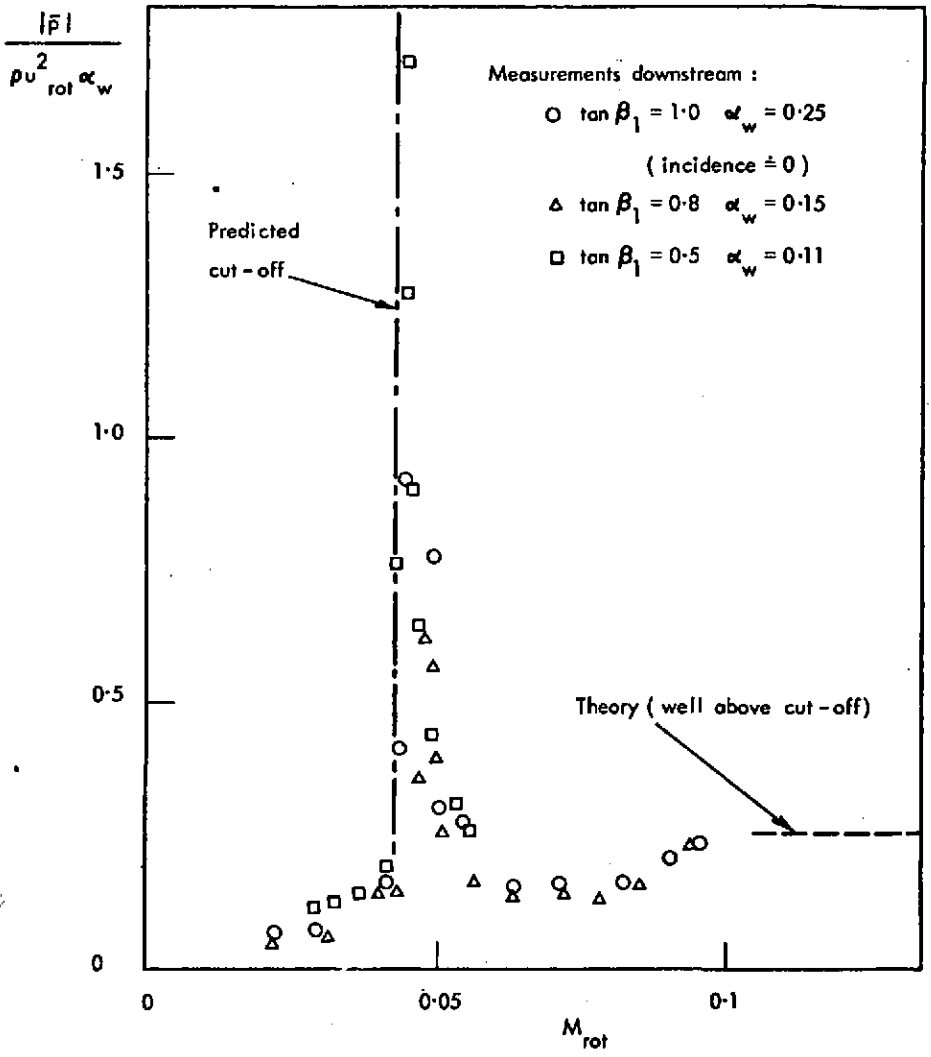
$\frac{|\bar{p}|}{\rho U_{rot}^2 \alpha_w}$
1·5
1·0
0·5
0
0
0·05
0·1
M_{rot}
Measurements downstream :
○ tan β_1 = 1·0 α_w = 0·25
(incidence ≐ 0)
△ tan β_1 = 0·8 α_w = 0·15
□ tan β_1 = 0·5 α_w = 0·11
Predicted
cut - off
Theory (well above cut - off)

Fig. 4

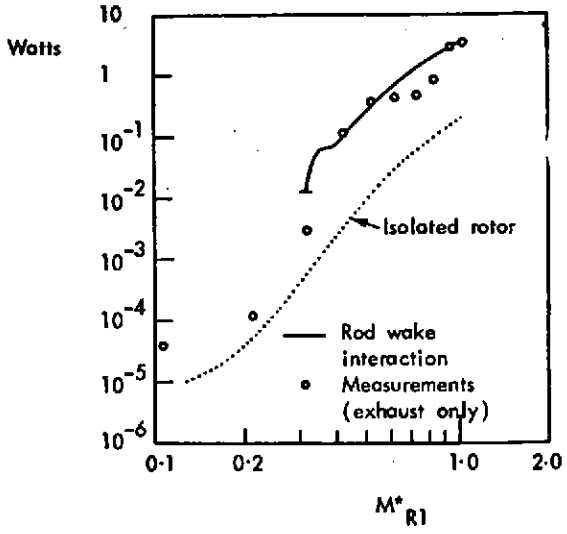
Watts
10
1
10^{-1}
10^{-2}
10^{-3}
10^{-4}
10^{-5}
10^{-6}
0·1
0·2
1·0
2·0
M^*_{R1}
Isolated rotor
Rod wake interaction
Measurements (exhaust only)

Fig. 5

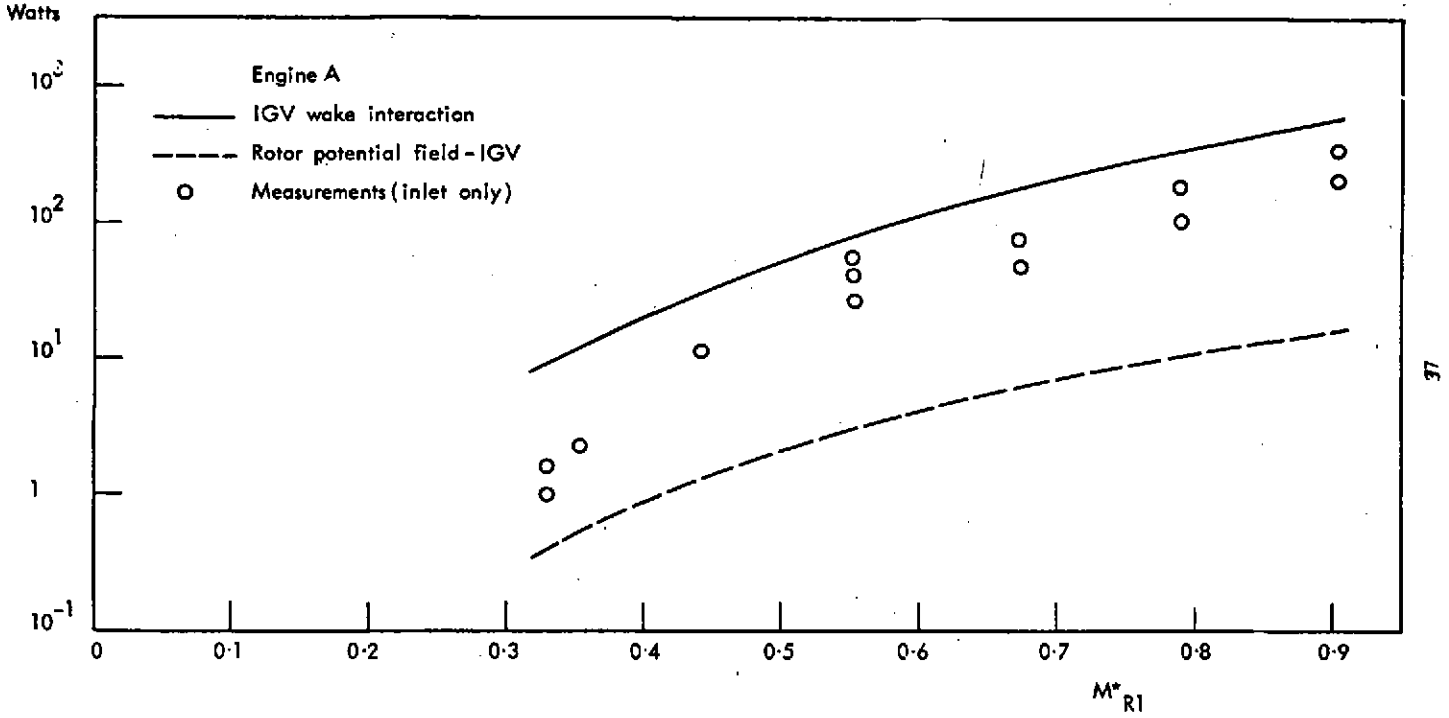
Watts
10^2
10^2
10^1
1
10^{-1}
Engine A
IGV wake interaction
Rotor potential field - IGV
Measurements (inlet only)
0
0·1
0·2
0·3
0·4
0·5
0·6
0·7
0·8
0·9
M^*_{R1}

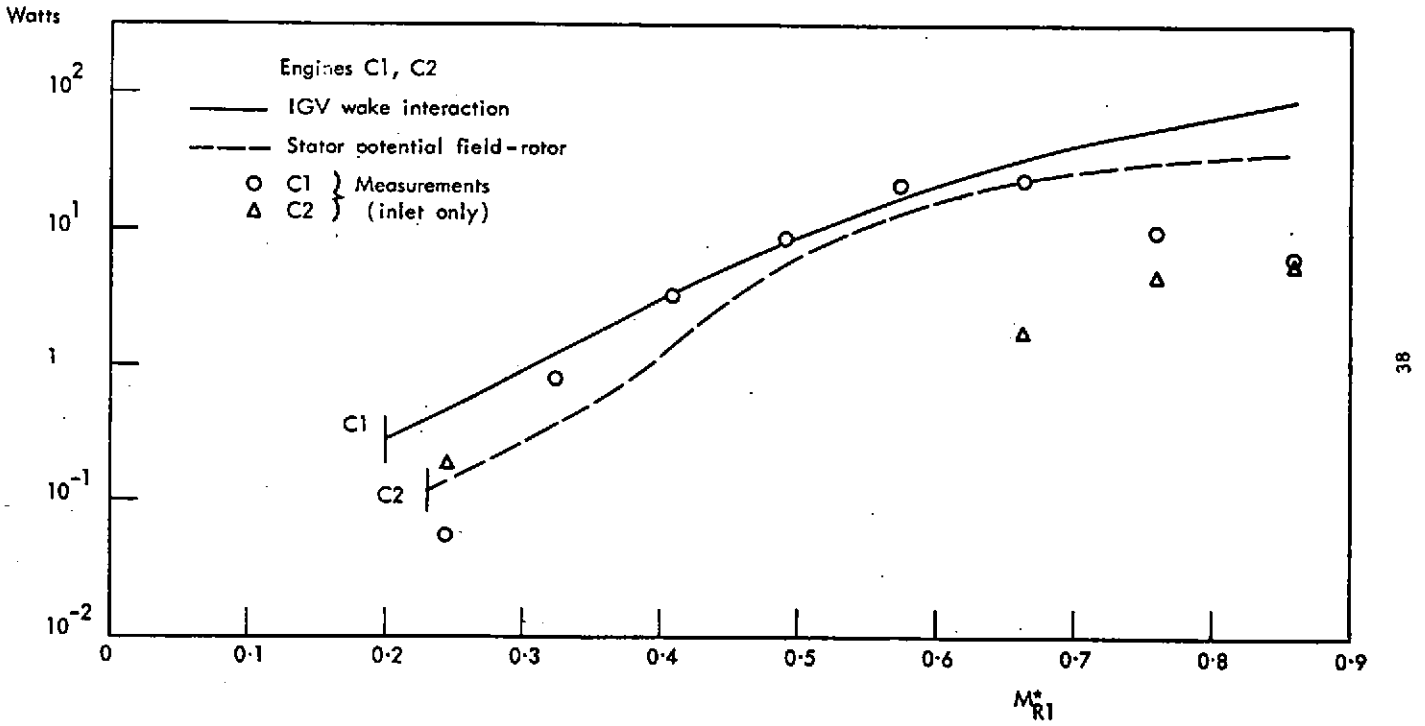
Watts
Engines C1, C2
IGV wake interaction
Stator potential field - rotor
C1 } Measurements
C2 } (inlet only)
10^2
10^1
1
10^{-1}
10^{-2}
C1
C2
0
0·1
0·2
0·3
0·4
0·5
0·6
0·7
0·8
0·9
M^*_{R1}

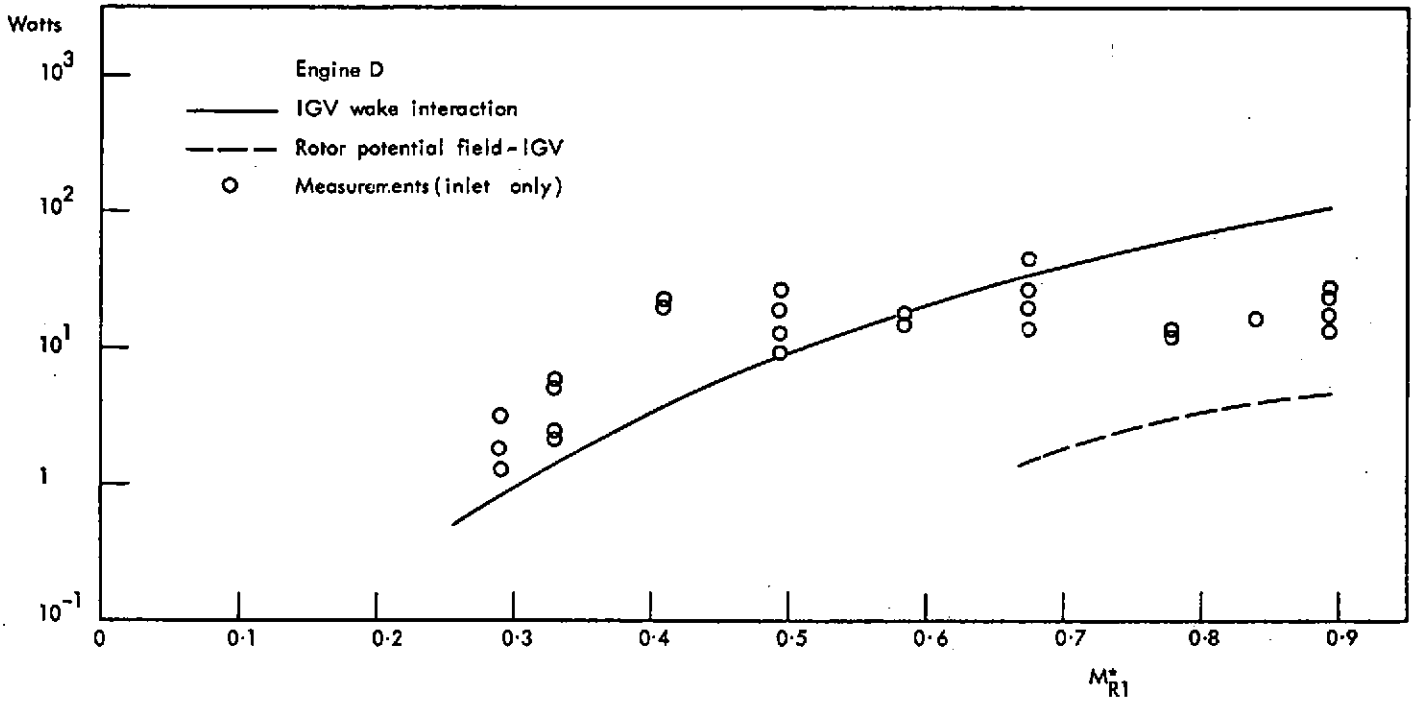
Watts
10^3
10^2
10^1
1
10^{-1}
Engine D
IGV wake interaction
Rotor potential field - IGV
Measurements (inlet only)
0
0·1
0·2
0·3
0·4
0·5
0·6
0·7
0·8
0·9
M^*_{R1}